

Article

Waste Management of Red Mud and Fly Ash to Utilize in Road Subgrade Material

Ali Sinan Soğancı, Yavuz Yenginar *, İlyas Özkan, Yusuf Güzel and Adnan Özdemir

Civil Engineering Department, Engineering Faculty, Necmettin Erbakan University, 42090 Konya, Türkiye; asoganci@erbakan.edu.tr (A.S.S.); iozkan@erbakan.edu.tr (İ.Ö.); yguzel@erbakan.edu.tr (Y.G.); adnanozdemir@erbakan.edu.tr (A.Ö.)

* Correspondence: yyenginar@erbakan.edu.tr

Abstract: Red mud (RM) is a waste material obtained during the production of aluminum from bauxite minerals. RM causes environmental pollution due to its high alkaline properties. Therefore, RM materials are stored in waste reservoirs. As production continues, the number of required waste reservoirs increases day by day. This study aims to utilize RM waste material in construction structures to contribute to the economy. The research investigates the potential use of RM waste material as road fill material. RM was improved using another waste material of fly ash (FA) since RM has low strength. Atterberg limit tests, compaction tests, unconfined compression tests, CBR tests, and SEM analyses were conducted on stabilized RM samples. In the physical properties of stabilized RM, Atterberg limits and optimum moisture content increase and density decreases since FA content increases. In the mechanical properties of stabilized RM, unconfined compressive strength, initial and secant modulus of elasticity, and California bearing ratio increase and maximum peak strain decreases since FA content and curing period increase. SEM images prove the increase in mechanical properties due to the cementation products (CSH and CAH gels) formed in the microstructure of stabilized RM. The results showed that RM waste stabilized with FA can be used as road subgrade material.

Keywords: fly ash; microstructure; red mud; road subgrade; stabilization; strength



Citation: Soğancı, A.S.; Yenginar, Y.; Özkan, İ.; Güzel, Y.; Özdemir, A. Waste Management of Red Mud and Fly Ash to Utilize in Road Subgrade Material. *Sustainability* **2024**, *16*, 2987. <https://doi.org/10.3390/su16072987>

Academic Editors: Jeongsoo Yu, Kazuaki Okubo and Xiaoyue Liu

Received: 3 March 2024

Revised: 22 March 2024

Accepted: 1 April 2024

Published: 3 April 2024



Copyright: © 2024 by the authors. Licensee MDPI, Basel, Switzerland. This article is an open access article distributed under the terms and conditions of the Creative Commons Attribution (CC BY) license (<https://creativecommons.org/licenses/by/4.0/>).

1. Introduction

Red mud is an industrial waste deployed after alumina extraction from bauxite during the most commonly used Bayer process. In the process of producing one ton of alumina, depending on the raw material provided, about 1 to 1.5 tons of red mud, also known as bauxite residue, are extracted [1–4]. Storage of the red mud waste has been made in a half-viscous form [5,6] or in a dry form in large embankment areas [7]. Increasing demand for alumina in line with the ever-growing industrial developments, there has been a 2.5% annual rise in alumina production in the past 20 years [8], therefore there has also been a rise in the red mud waste generated. In other words, in 1990, the production of alumina was about 19 million tons, and this amount reached 58 million tons in 2015 and rose to 90 million tons by 2021 [9].

Besides the massive disposal of the red mud requiring reservoirs in great volumes, the composition of the red mud is also problematic from the environmental perspective and the disposed land cannot be used for construction or agriculture when it is abandoned [10,11]. The main compositions of red mud include Fe_2O_3 , Al_2O_3 , SiO_2 , Na_2O , and CaO , and small amounts of Zr, Y, Th, and U elements [12]. These components and elements of the red mud feature serious environmental problems. Namely, high alkalinity (with pH higher than 11), the inclusion of heavy metals, as well as radioactive elements are regarded as the main causes of groundwater as well as air pollution [13–15]. In addition, storing vast amount of red mud can lead to failures of reservoirs as experienced in Ajka, Hungary when the red mud with a pH of approximately 12 flowed in 2010, killing 10 people and injuring many in hundreds, and destroying around 40 km² of farmland [16,17]. A similar disaster

occurred in 2018 in the Para state of Brazil due to the heavy rainfall. Soil contamination with high volumes of lead, aluminum, and sodium has threatened the water resources and agriculture of the local area [18].

Considering the environmental impacts of red mud, there has been ongoing research aiming to make industrial waste useful rather than having to store it at large scales. For instance, in order to neutralize red mud, some research suggested mixing it with seawater, acidic leachates in mine plants, bioremediation, and carbonization [19,20]. Moreover, red mud was aimed to be used in making bricks and glass metals [2,21,22]. Moreover, red mud has been utilized as a catalyst in hydrodechlorination reactions and miscellaneous reactions and in biodiesel productions [23–25]. Red mud has also been demonstrated to be an alternative or partial substitute for cement due to its alumina silicate content and pozzolanic reactions [22,26,27]. In some research, red mud is used for co-pyrolysis of non-metallic fractions of waste printed circuit boards [28] and the production of a bio-magnetic adsorbent [29]. Red mud is also used to produce geopolymer materials with fly ash and sodium silicate [30]. Red mud was mixed with different percentages of blast furnace slag and sodium silicate solution, and high compressive strength values, up to 50 MPa, were obtained [31].

In the construction of the road base and sub-base, either the filling material (sand, gravel) has appropriate gradation is placed by compaction or the existing soil is improved with additive materials. The most preferred additive materials in soil improvement are cement [32,33], lime [34,35], and fly ash [36,37]. Additionally, red mud has been tested to be suitable in road foundations, as the required unconfined compressive strength ranges from 1.38 MPa to 5.17 MPa [38]. In this regard, red mud was involved in road base construction at different percentages with aggregate, flue gas desulfurization fly ash, Calcium Oxide admixture (as a binder), and cement [15]. It was demonstrated that the use of up to 35% of red mud can give sufficient compressive strength, of up to 6 MPa, required for the road base. In addition, from unconfined compressive test (UCS), splitting tensile strength (STS), and California bearing ratio (CBR) test results, the performances of red mud mixing with ground granulated blast furnace slag (GGBS) have shown to be appropriate in building and road foundations and runways [39]. The admixtures of GGBS from 5 to 25 percentage ranges of red mud caused the increase in the UCS, STS, and CBR values from 0.394 MPa to 1.608 MPa, from 0.042 MPa to 0.237 MPa, and from 5 to 25%, respectively, at 7 days of curing time. When the amount of GGBS inclusion was above 25%, the values were shown to be reduced. A combination of cement, phosphogypsum, and organic polymer modifiers was also added to the red mud at different percentages [40]. After 7 days of curing, the red mud including 10 to 12 percent of the modifier reached around 5 MPa of confined strength. However, when the red mud specimens with different percentages of modifiers were immersed in water for one day, the UCS values were reduced significantly. The least reduction happened in the 8% inclusion of modifier, as shown to be the optimum modifier level involvement in red mud. Red mud was also been functioned with loess soil benefitted road bases [41]. From UCS of the different proportioned mixtures at 7 days curing time, 15% or 20% of red mud contents led to the highest two UCS values of 2.19 MPa and 2.39 MPa, respectively. In literature, several more similar studies have investigated the mechanical properties of red mud with and without admixture materials (hydrate lime, gypsum, cement kiln dust, and fly ash, etc.) and expressed the prospect of red mud used in the construction of road bases [14,42–45].

To the best of the authors' knowledge, there is no study in which red mud alone has been used as a road base material by improving it with fly ash. In this study, red mud obtained from Etibank Seydisehir Aluminum Plant in Konya, Turkey is studied regarding its possible application in road base construction. Then, red mud is stabilized with fly ash at different percentages. Firstly, the red mud reservoir is presented. Later, the gradation and Atterberg limits of the red mud and mixes are determined. Optimum moisture content, unconfined compression strength, and California Bearing ratio of stabilized red mud samples are determined at different curing ages.

2. Materials and Methods

2.1. Materials

In the present study, waste materials were provided from Eti Aluminum Factory (Seydişehir, Konya, Turkey). The factory has a bauxite processing capacity of 500,000 tons per year. As a result of the processing of bauxite, 500,000–750,000 tons of red mud (RM) waste is generated annually. RM waste is stored in tailings dams around the factory. Until the last decade, RM slurry had 30% solids pumped into tailings dams. However, in order to use the dam capacities efficiently, the RM sludge released during bauxite processing was compressed in press filters, and the solid ratio was increased to 70%. Three dams have been constructed in the last fifty years and the storage of RM material poses an environmental and economic problem. The factory meets its energy needs from natural gas and coal. As a result of the combustion of coal, fly ash (FA) waste is produced. FA waste is used to fill some of the gallery spaces in coal mines. This study aimed to produce high-performance filling material by improving the physical, mechanical, and mineralogical properties of RM waste stabilized with FA.

2.1.1. Red Mud

RM mostly consists of silt-sized grains (Figure 1). The uniformity coefficient of RM (D_{60}/D_{10}) is determined as 5.75 since D_{60} and D_{10} are the grain size of RM corresponding to 60% and 10% percent finer, respectively. Maximum grain diameter of RM (D_{max}) is 0.3 mm. According to the consistency limits, the plasticity index of RM is low (3.5%). The soil class of RM is low plasticity silt (ML) according to the Unified Soil Classification System (USCS) [46]. The physical and mechanical properties of RM are given in Table 1. Due to the chemical composition obtained by XRF analysis, the sum of the Si, Al, and Fe oxides in RM is close to 50% and it also contains 25.1% CaO (Table 2). The red mud powder displays diverse morphologies, with certain individual particles appearing as flakes and others as spherical particles (Figure 2). The amount of organic matter in RM is below detection limits [47,48]. The absence of organic matter also restricts plant growth on bauxite residue [46]. In addition, the very fine particles might be associated with sodium/aluminum minerals within the RM powder. Conversely, the larger particles could potentially be attributed to iron mineral groups or unaltered minerals present in the bauxite ore.

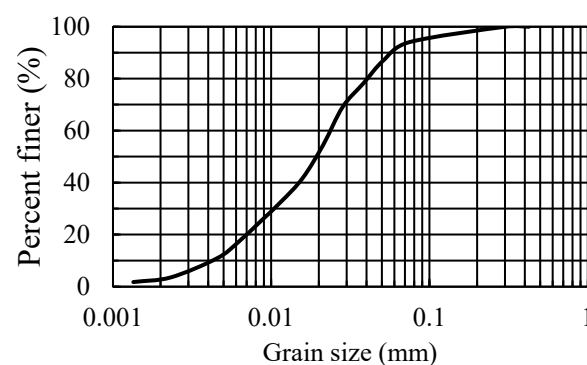


Figure 1. Grain size distribution of red mud.

Table 1. The physical and mechanical properties of RM.

Property	Value
Specific gravity	2.56
Liquid limit, LL (%)	40.5
Plastic limit, PL (%)	37
Plasticity index, PI (%)	3.5
Soil class (USCS)	ML
Optimum moisture content, OMC (%)	34
Maximum dry density, MDD (g/cm^3)	1.41
Unconfined compressive strength ^a (kPa)	220

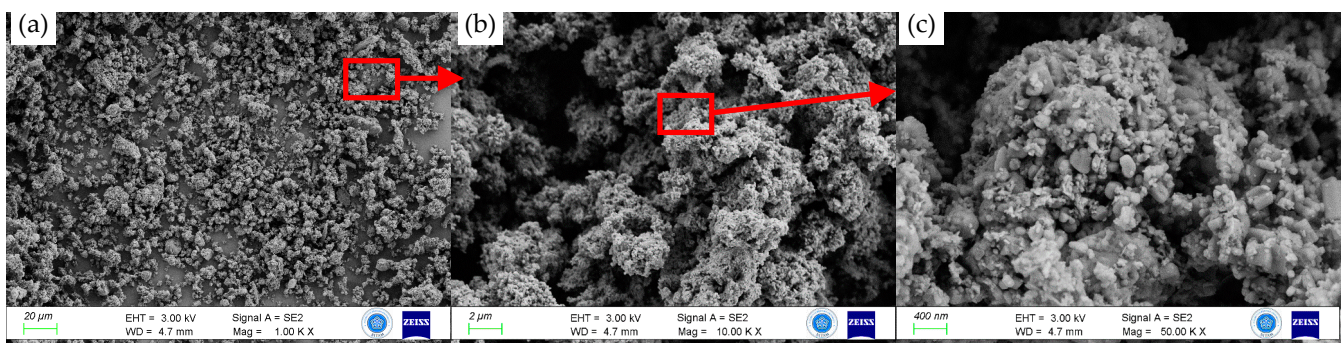
Table 1. Cont.

Property	Value
CBR swell ratio (%)	1.3
CBR dry (%)	4.15
CBR wet (%)	2.85

^a The remolded RM sample has OMC and MDD.

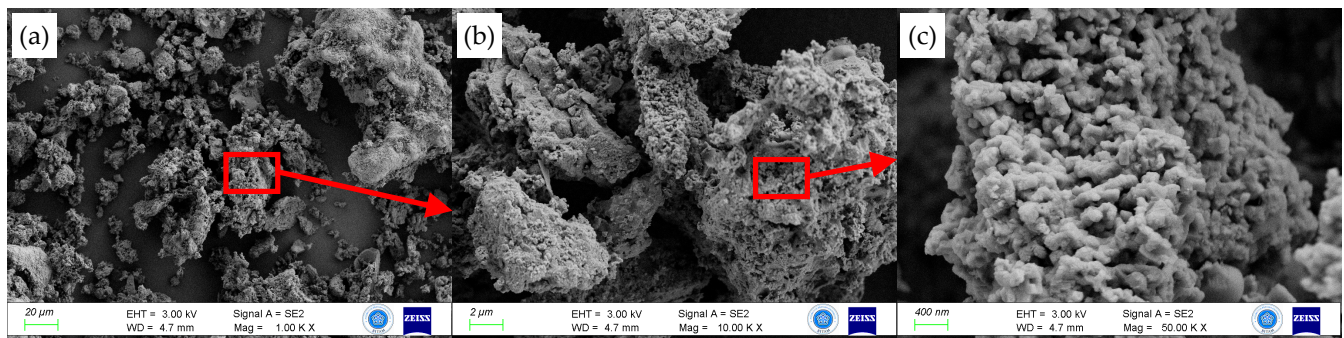
Table 2. The chemical composition of waste materials.

Material	Al ₂ O ₃	SiO ₂	Fe ₂ O ₃	CaO	Na ₂ O	TiO ₂	ZrO ₂	SO ₃	MgO	K ₂ O
RM (%)	14.30	11.40	24.10	25.10	9.35	2.95	0.44	0.28	0.22	0.11
FA (%)	5.10	15.50	8.09	41.80	-	0.42	0.40	16.50	1.20	0.60

**Figure 2.** SEM images of RM: (a) MF = 1000, (b) MF = 10,000, and (c) MF = 50,000.

2.1.2. Fly Ash

FA obtained from Eti Aluminum Factory is a finer material than RM (Figure 1). In the chemical composition of FA, SiO₂ + Al₂O₃ + Fe₂O₃ is 23.59% and SO₃ content is 16.5%. In the previous version of ASTM C618-17 [49], it is required that SiO₂ + Al₂O₃ + Fe₂O₃ > 50% for C class FA and SiO₂ + Al₂O₃ + Fe₂O₃ > 70% for F class FA. In addition, the limit of SO₃ content is 5% for all types of FA. In the latest version of ASTM C618 [50], however, the unburned lime (CaO) content is the most significant factor in classifying fly ash. A fly ash is classified as F class if CaO ≤ 18%; otherwise, it is C class (CaO > 18%). The FA is categorized as “Class C” according to its chemical composition since CaO content is 41.8%. Therefore, the C class FA has pozzolanic and self-cementing properties. FA grains have irregular geometries of various dimensions due to the SEM image (Figure 3).

**Figure 3.** SEM image of FA: (a) MF = 1000, (b) MF = 10,000, and (c) MF = 50,000.

2.2. Methodology

The physical and mechanical properties of RM material are insufficient to use a fill material of either pavement or highway. Therefore, RM material may be used as fill material

after a stabilization process with a chemical additive material. C class FA was preferred for the stabilization process.

RM obtained from the factory was plastic state and had approximately 30% water content (Figure 4a). RM was firstly dried at 105 °C for 24 h. Then, it was crumbled and pulverized with a hammer (Figure 4b). Finally, RM material was sieved from No. 40 sieve to use an experimental process.

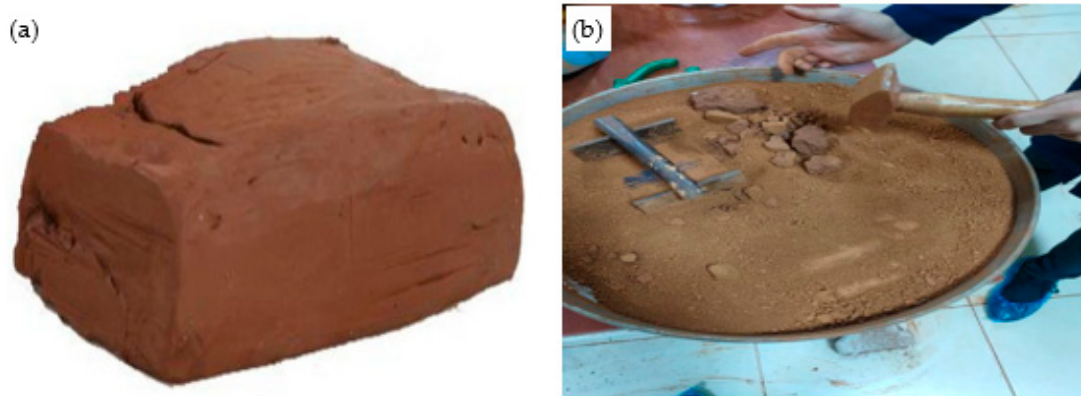


Figure 4. The images of red mud: (a) plastic state and (b) powder form.

In the stabilization process, the FA content was determined based on the existing literature studies. For instance, the optimum FA content in soil stabilization was 9–12% [51] and 25% [52,53]. Therefore, the FA ratio was selected between 5% and 25% by the dry weight of the mix (Table 3). Before each experimental testing stage, RM and FA were mixed with a spatula in a dry form. Then, the materials were sieved two times through a No.40 sieve to obtain a homogeneous mixture at each mixture. The testing methodology intends to investigate the consistency, compaction, strength (UCS, CBR), and microstructural (SEM) characteristics of RM stabilized with FA.

Table 3. The dry weight percentages of RM and FA in stabilized specimens.

Stabilized Specimen	RM (%)	FA (%)
RM+5% FA	95	5
RM+10% FA	90	10
RM+15% FA	85	15
RM+20% FA	80	20
RM+25% FA	75	25

Consistency limits play a crucial role in determining soil classification and plastic properties for fine-grained materials like red mud and fly ash. The consistency properties of freshly mixed RM–FA–water combinations were investigated by Atterberg limit tests [54].

Maximum dry density (MDD) and optimum moisture content (OMC), critical parameters for engineering tests, were determined from the standard Proctor test [55], as the stabilized specimen is generally compacted at MDD and OMC conditions in the field. In the Proctor test, RM or RM+FA mixtures were placed inside the mold (diameter of 10.16 cm and height of 10.5 cm) as 3 layers and were compressed at 25 drops/layer by a 2.5 kg hammer. Since the RM or RM+FA mixtures generally contain silt, over-granulation is not observed during sample preparation. Additionally, after mixing with water, any few formed clumps were crushed to achieve a homogeneous distribution of water in the mixture. Compaction tests were performed for each mixture to decide the most durable condition of the stabilized specimen. In addition, the bulk density of each stabilized specimen was determined at the optimum situation.

The unconfined compressive strength (UCS) test, conducted initially due to its brief duration and ability to provide insight into specimen behavior and strength, aims to establish

strength characteristics. The UCS test samples were prepared due to the compaction test results of each mixture. Firstly, any mixture that has OMC and MDD was compressed in the compaction mold following the ASTM D698 [55] standard. Secondly, cylindrical samples were obtained by pushing steel tubes (50 mm in diameter and 100 mm in height) into the compressed mixture. Steel tubes were lubricated before sampling to obtain an undisturbed sample. Then, the stabilized soil sample was removed from the steel tube, bagged, and left to cure. In laboratory conditions, all the specimens were cured in a desiccator maintaining 95% humidity. Curing periods were 7, 28, and 56 days. At the end of the curing periods, the UCS test was performed according to ASTM D2166 [56]. The loading capacity of the UCS machine was 50 kN, and it was capable of constant loading speed. Loading speed during the tests was 1 mm/min, corresponding to 1%/min axial strain rate and compatible with the ASTM standard (0.5–2%/min strain rate). Stress and strain data were recorded until the failure of the stabilized specimen or the axial strain of at most 15%. UCS tests were performed on three samples for each mixture and curing period. An average of them presented as unconfined compressive strength (q_u).

The primary objective of this study is to utilize RM as fill material in highway and road applications. The California Bearing Ratio (CBR) is the most sensitive parameter for evaluating subgrade, subbase, and base materials in the design of pavements. Test specimens (RM or RM+FA) were compacted at 100% MDD and OMC in a mold (152.4 mm in diameter and 177.8 mm in height) following the ASTM D698 standard. In the wet CBR test, the compacted specimen was allowed to soak for 96 h, then the loading stage was started. The load and displacement data were recorded during the loading stage since the loading rate was 1.27 mm/min. The CBR is the ratio of the unit load required to penetrate 2.54 mm and 5.08 mm of the test material to the unit load required to penetrate a standard material of well-graded crushed stone [57].

The microstructural characteristics of the unstabilized and stabilized samples were performed by scanning electron microscope (SEM) imaging in a ZEISS EVO LS10 field emission machine (Zeiss Microscopy, Oberkochen, Germany). After 56 days of curing time, a $1 \times 1 \times 1 \text{ cm}^3$ piece was taken from the shear surfaces of UCS test samples and SEM images were obtained by different magnifications. The CBR and SEM analyses were performed on untreated RM and the stabilized specimen exhibiting the highest strength according to UCS tests.

3. Results and Discussions

3.1. Atterberg Limits

The liquid limit, plastic limit, and plasticity index values of RM are 41.6, 32.8, and 8.8, respectively. These values exhibit similarity with the study conducted by Chandra and Krishnaiah [58]. They reported liquid limit, plastic limit, and plasticity index values for red clay as 39%, 28%, and 11%, respectively. As the FA replacement ratio increases, the Atterberg limits of the stabilized RM increase. At the 25% FA content, the liquid limit, plastic limit, and plasticity index increase by 26.5%, 21.0%, and 47.1%, respectively (Figure 5). RM mostly contains silt-sized grains. FA is a fine material and has a higher water absorption capacity than RM. Therefore, the increasing amount of FA increases the consistency limits of stabilized RM. This situation affects the soil class of the freshly mixed RM-FA-water mixture. According to the consistency limits of the mixes, RM, RM+5%FA, RM+10%FA, and RM+15%FA are classified as ML, while RM+20%FA and RM+25%FA are classified as MH.

3.2. Compaction Characteristics

The optimum moisture content (OMC) and the maximum dry density (MDD) of RM were 28.1% and 1.466 g/cm^3 , respectively. These values exhibit similarities with the studies conducted in the literature. For instance, Chandra and Krishnaiah [58] reported the OMC and MDD values for red clay as 34.39% and 1.59 g/cm^3 , respectively. The difference arises from the clay content in the red mud samples. The red mud that they used exhibits more plastic characteristics compared to the red mud in Turkey. As the amount of FA added to the RM increases, MDD decreases, and OMC increases (Figure 6). When 25% FA was added

to the RM, OMC increased by 8.8% (30.6%) and MDD decreased by 8.4% (1.343 g/cm³). FA increases the water needs of the mixture. During the compaction test, the amount of water required for the RM and FA grains to be arranged in the most suitable grain arrangement (less void) increases depending on the FA content. As the amount of FA in the unit volume of the stabilized material increases, MDD decreases due to the decrease in RM mass and increase in water mass. The specific densities of RM, FA, and water are 2.67, 2.18, and 1, respectively. The MDD decreases due to the density difference of the materials and the increase in the amount of water per unit volume.

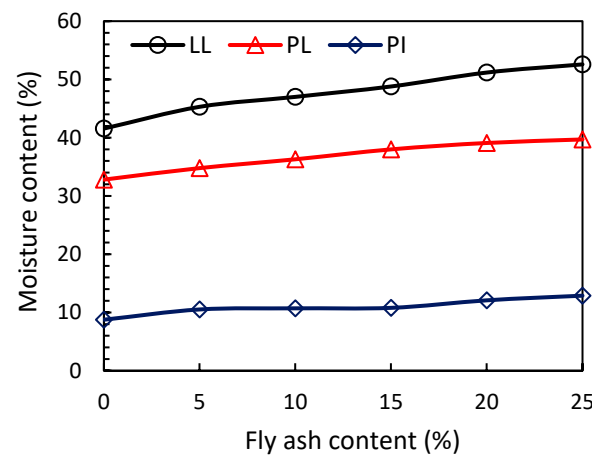


Figure 5. Atterberg limits of stabilized red mud.

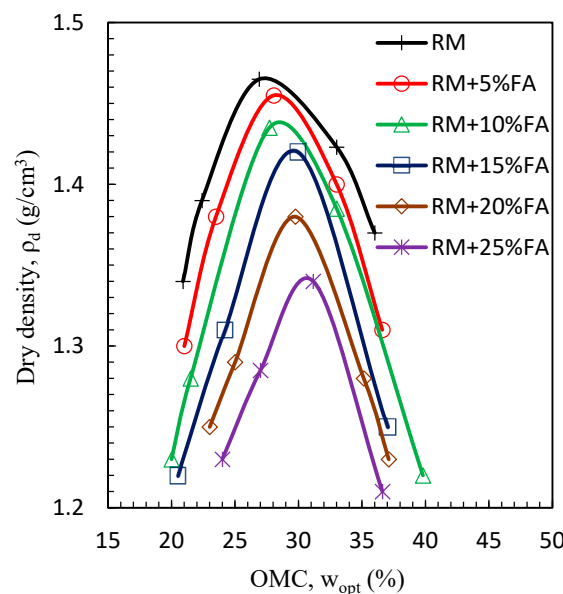


Figure 6. Compaction characteristics of stabilized red mud.

3.3. Density

After mixing the RM with FA in different ratios, they were compacted at optimum moisture content, and then their bulk densities were determined. The bulk density of the improved soil affects the physical and mechanical properties of a composite material consisting of RM, FA, and water. In addition, if the improved soil is used as a filling material, the weight of the filling affects the settlements in the ground under the filling. The bulk density of RM is 1.878 g/cm³. When the RM is stabilized with 5–25% FA, the bulk density ranges from 1.865 to 1.754 g/cm³ (Figure 7). The bulk density decreases as the FA content added to the RM increases. While the bulk density decreased by 2% for the 15% FA replacement ratio, the decrease was 6.6% in the 25% replacement ratio. A sharp decrease in

bulk density occurs when the RM is stabilized with more than 15% FA, indicating that FA dominates the stabilized RM behavior. The reason for the decrease in bulk density is the grain density of FA is less than RM.

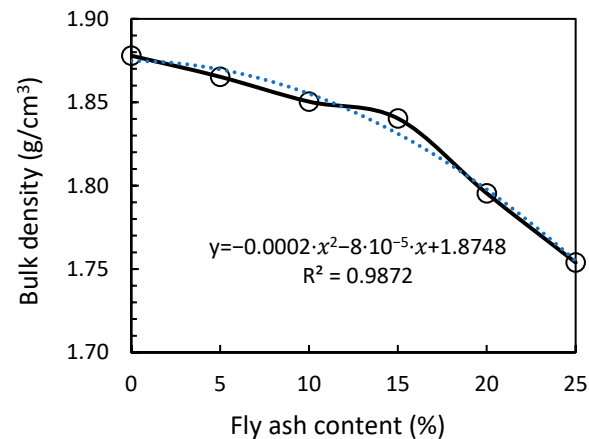


Figure 7. Bulk density of stabilized red mud.

3.4. Unconfined Compressive Strength (UCS) Characteristics

The stress–strain curves of red mud specimens stabilized with fly ash are given in Figure 8a,b with respect to curing periods. The unconfined compressive strength of red mud specimens increases with the amount of fly ash. Although red mud specimens are generally composed of silt particles, the unconfined compressive strength of these specimens with fly ash additives increases with both the additive ratio and the curing periods. Another important output derived from Figure 8a,b is that red mud specimens with fly ash additives become more brittle with the curing period.

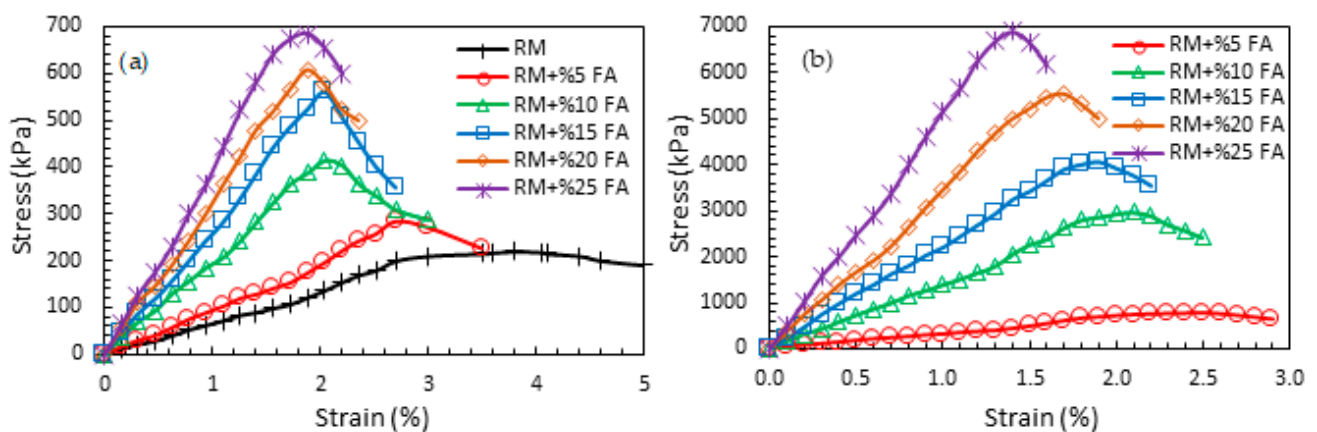


Figure 8. Stress–strain curves of red mud specimens stabilized with fly ash: (a) without curing and (b) after 56 days of curing.

The UCS values of red mud samples improved with fly ash are presented in Figure 9. Additionally, the effect of curing periods is depicted in the figure. The increase in the amount of fly ash has resulted in an enhancement of the strength of red mud samples. Furthermore, an increase in the curing period further elevates the improvement rates in the red mud samples.

In this study, the values of both the initial tangent modulus (E_0) and the secant modulus (E_{50}) of red mud samples improved with fly ash are given in Figure 10. The effects of both the curing period and the amount of fly ash additive on the variations in these two moduli have been investigated.

The strength of the red mud specimens improved with the addition of fly ash. The increase in strength in the treated samples resulted in both an increase in initial tangent

modulus and secant modulus. The increase in both modulus values was significantly influenced by the curing period. When the curing period and the amount of fly ash are compared, it is evident that the curing period is more effective than the other.

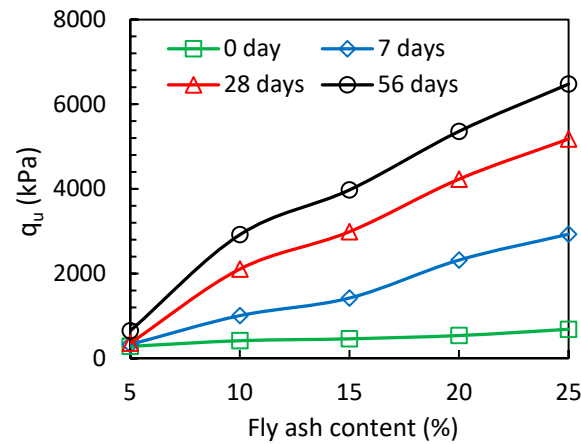


Figure 9. The values of UCS of stabilized specimens.

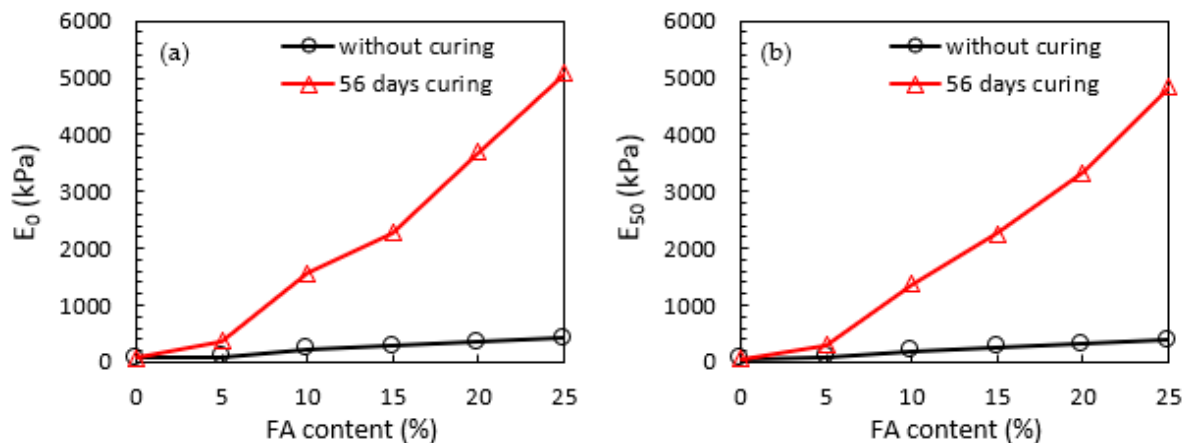


Figure 10. (a) Initial tangent modulus and (b) secant modulus of red mud specimen stabilized with fly ash.

Consequently, this increase in the unconfined compressive strength of red mud specimens with fly ash additives can be explained by pozzolanic reactions. In this improvement method, the presence of pozzolanic reactions will be investigated in the SEM analysis.

3.5. California Bearing Ratio (CBR)

Both dry and soaked CBR tests were conducted on the red mud sample. Load-penetration curves obtained from both dry CBR and wet CBR tests were drawn in Figure 11.

The standard load corresponding to 100% CBR value (for ballast material) is 13.34 kN for 2.5 mm penetration and 20.01 kN for 5.0 mm penetration. The CBR value of a material is the greater of the ratio of the test loads to the relevant standard loads corresponding to 2.5 and 5.0 mm penetrations. As a result of the dry CBR test, the dry CBR value was calculated as 4.15%. Following the dry CBR test, a wet CBR test was performed. After soaking the red mud sample in water for 4 days, the CBR swelling value was measured as 5.3%. Subsequent to the soaking phase, the CBR value decreased from 4.15% to 2.85% as a result of the wet CBR test. Due to the presence of a certain amount of clay in the red mud, a degree of swelling and a reduction in strength occurred during the wet CBR test. Consequently, it was observed that conducting wet CBR tests on the modified samples is more appropriate.

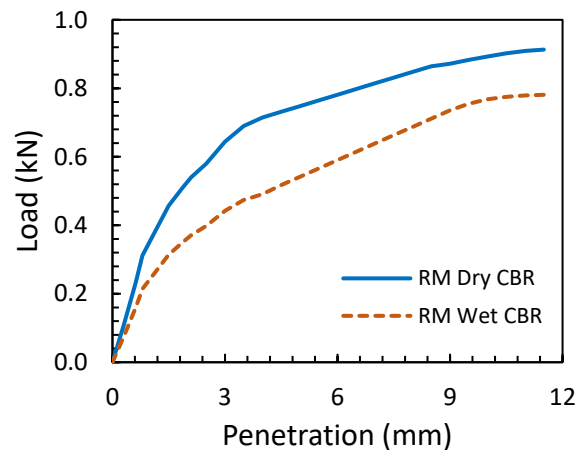


Figure 11. Load-penetration curves of red mud specimens obtained from CBR tests.

The values obtained at the end of the study demonstrate similarities with the results of previous studies. Chandra and Krishnaiah [58] reported that the CBR values of RM were 5.48% for the unsoaked sample and 1.56% for the soaked sample.

After the unconfined compression test, the samples with the highest strength (RM+25% FA) underwent wet CBR testing. The selected samples were compacted into the CBR mold at maximum dry density and optimum water content. The compacted samples were intended to be cured for 56 days. However, due to significant hardening of this specimen within the mold after 28 day curing period, it was decided to proceed with the testing phase. The modified red mud samples waited in the humid room for 28 days. Then this specimen was soaked in water for 4 days and no volume expansion (swelling) was observed during this process. The stable volume of the CBR samples is attributed to the fact that the red mud gained strength during the curing period through the incorporation of additives. Following the soaking process, the loading phase was initiated. The load–displacement graph during the loading phase is presented in Figure 12.

The red mud samples modified with fly ash additives exhibited brittle material characteristics. These samples underwent displacement of up to 4.5 mm at most, after these specimens promptly fractured. The CBR value of this specimen was calculated as 268.25%. This value is significantly higher than the desired CBR value for road fill materials. According to the Technical Specification of Highways in Turkey [59], for improved fill soils, the unsoaked CBR value should be greater than 15%, and the CBR swelling value should be less than 2. This improved specimen is a suitable embankment material with respect to the Technical Specification of Highways in Turkey.

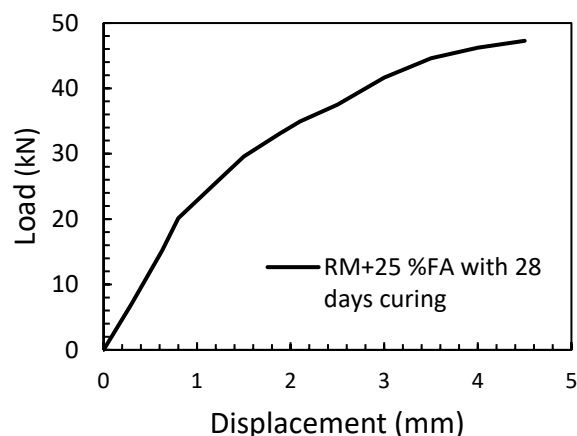


Figure 12. The load–displacement graph of RM+25% FA with 28 days curing.

3.6. SEM Characteristics

The SEM images of RM stabilized with 25% FA at 56 days of curing time are presented in Figure 13. Different hydration products were seen in SEM images taken at different magnification factors (MF). Calcium aluminate hydrate (CAH), ettringite (AF_m), and calcium silicate hydrate (CSH) products are clearly visible in the SEM images, where the MF is 10,000, 25,000, and 50,000, respectively. Cation exchange and hydration reactions begin when RM, FA, and water are mixed. CaO and SiO₂ contained in RM and FA materials react with water to form CSH gel and calcium hydroxide (Ca(OH)₂). In addition, CaO, Al₂O₃, SO₃ compounds in the environment form the AF_m compound (Ca₂(Al,Fe)(OH)₆]₂·X·nH₂O). Ca(OH)₂ in the environment reacts again with SiO₂ and Al₂O₃ in RM and/or FA, forming CSH and CAH gels. CAH gel has the appearance of a thick and nonporous plate with dimensions of 2–10 μm. AF_m has an elongated cylindrical rod-shaped appearance and a length of 2–3 μm. CSH gels, on the other hand, have a curved and porous structure similar to honeycomb in very small sizes (~50 nm). Especially CSH and CAH gels cause the RM+FA mixture to gain high strength.

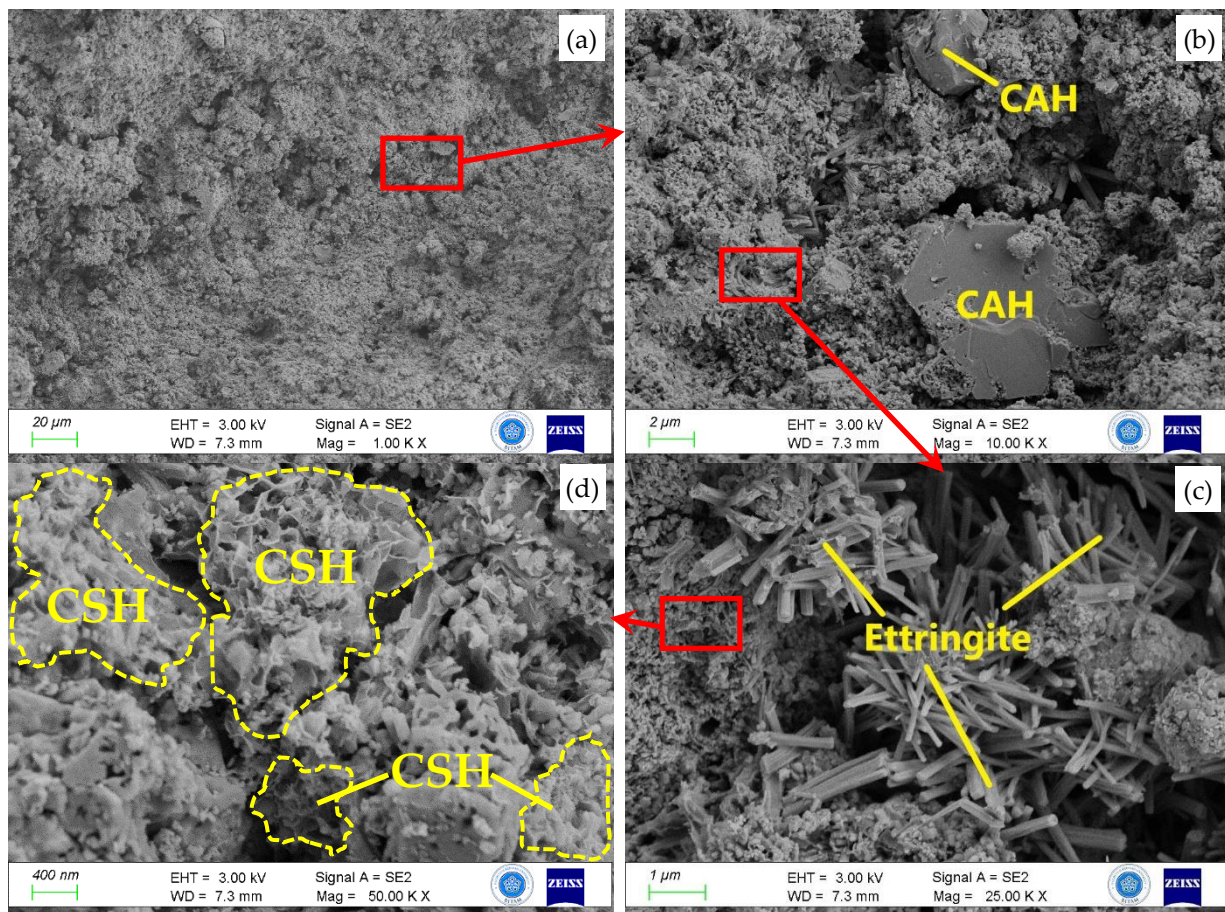


Figure 13. SEM images of RM+25%FA at 56 days of curing: (a) MF = 1000, (b) MF = 10,000, (c) MF = 25,000, and (d) MF = 50,000.

4. Conclusions

In this study, an industrial waste material, red mud, was attempted to be improved using another industrial waste material, fly ash. The findings obtained from the conducted experimental work and analyses have been summarized below.

- The lower density of fly ash compared to red mud, along with its finer particles, leads to an increase in plastic properties and optimum water content in the improved samples. However, it also results in a decrease in maximum dry density.

- The addition of fly ash to the red mud has increased the UCS strength. During the curing period, pozzolanic reactions took place, leading to a significant increase in the improvement percentage.
- According to the results of the wet CBR test, the CBR value for the red mud sample improved with 25% fly ash and cured for 28 days was found to be 268.25%. This value is more than sufficient for road fill material.

As a result of this study that was aimed to improve red mud with fly ash, it has been concluded that red mud can be utilized as a road fill material.

Author Contributions: Conceptualization, A.S.S., Y.Y. and İ.Ö.; Funding acquisition, A.S.S.; Investigation, Y.Y. and Y.G.; Methodology, Y.Y. and İ.Ö.; Project administration, A.S.S.; Resources, İ.Ö. and Y.G.; Supervision, A.Ö.; Validation, Y.G.; Visualization, Y.Y.; Writing—original draft, Y.Y. and İ.Ö.; Writing—review and editing, Y.Y. and A.Ö. All authors have read and agreed to the published version of the manuscript.

Funding: This research was funded by the Necmettin Erbakan University Scientific Research Projects Coordination Office (Grant No.: 221219002).

Institutional Review Board Statement: The study did not require ethical approval.

Informed Consent Statement: Not applicable.

Data Availability Statement: Data are contained within the article.

Conflicts of Interest: The authors declare no conflicts of interest. The funders had no role in the design of the study; in the collection, analyses, or interpretation of data; in the writing of the manuscript; or in the decision to publish the results.

References

1. Kumar, S.; Kumar, R.; Bandopadhyay, A. Innovative methodologies for the utilisation of wastes from metallurgical and allied industries. *Resour. Conserv. Recycl.* **2006**, *48*, 301–314. [[CrossRef](#)]
2. Yang, Y.; Wang, X.; Wang, M.; Wang, H.; Xian, P. Iron recovery from the leached solution of red mud through the application of oxalic acid. *Int. J. Miner. Process.* **2016**, *157*, 145–151. [[CrossRef](#)]
3. Hooda, A.; Malik, P.; Sangwan, V. Research paper on gauging engineering properties of red mud-fly ash-marble dust amalgamation. *Int. J. All Res. Educ. Sci. Methods* **2016**, *5*, 252–258.
4. Kehagia, F. A successful pilot project demonstrating the re-use potential of bauxite residue in embankment construction. *Resour. Conserv. Recycl.* **2010**, *54*, 417–421. [[CrossRef](#)]
5. Li, L.Y. Properties of red mud tailings produced under varying process conditions. *J. Environ. Eng.* **1998**, *124*, 254–264. [[CrossRef](#)]
6. Newson, T.; Dyer, T.; Adam, C.; Sharp, S. Effect of structure on the geotechnical properties of bauxite residue. *J. Geotech. Geoenviron. Eng.* **2006**, *132*, 143–151. [[CrossRef](#)]
7. Power, G.; Gräfe, M.; Klauber, C. Bauxite residue issues: I. Current management, disposal and storage practices. *Hydrometallurgy* **2011**, *108*, 33–45. [[CrossRef](#)]
8. Silveira, N.C.G.; Martins, M.L.F.; Bezerra, A.C.S.; Araújo, F.G.S. Red mud from the aluminium industry: Production, characteristics, and alternative applications in construction materials—A review. *Sustainability* **2021**, *13*, 12741. [[CrossRef](#)]
9. U.S. Geological Survey. *Mineral Commodity Summaries 2022*; USGS: Reston, Virginia, 2022.
10. Tsakiridis, P.E.; Agatzini-Leonardou, S.; Oustadakis, P. Red mud addition in the raw meal for the production of Portland cement clinker. *J. Hazard. Mater.* **2004**, *116*, 103–110. [[CrossRef](#)]
11. Liu, W.; Chen, X.; Li, W.; Yu, Y.; Yan, K. Environmental assessment, management and utilization of red mud in China. *J. Clean. Prod.* **2014**, *84*, 606–610. [[CrossRef](#)]
12. Kalkan, E. Utilization of red mud as a stabilization material for the preparation of clay liners. *Eng. Geol.* **2006**, *87*, 220–229. [[CrossRef](#)]
13. Balomenos, E.; Gianopoulou, I.; Pnias, D.; Paspaliaris, I. A novel red mud treatment process: Process design and preliminary results. *Travaux ICSOBA* **2011**, *36*, 255–266.
14. Deelwal, K.; Dharavath, K.; Kulshreshtha, M. Evaluation of characteristic properties of red mud for possible use as a geotechnical material in civil construction. *Int. J. Adv. Eng. Technol.* **2014**, *7*, 1053.
15. Mukiza, E.; Liu, X.; Zhang, L.; Zhang, N. Preparation and characterization of a red mud-based road base material: Strength formation mechanism and leaching characteristics. *Constr. Build. Mater.* **2019**, *220*, 297–307. [[CrossRef](#)]
16. Gelencsér, A.; Kováts, N.; Turóczy, B.; Rostási, Á.; Hoffer, A.; Imre, K.; Nyirő-Kósa, I.; Csákberényi-Malasics, D.; Tóth, Á.; Czitrovszky, A.; et al. The red mud accident in Ajka (Hungary): Characterization and potential health effects of fugitive dust. *Environ. Sci. Technol.* **2011**, *45*, 1608–1615. [[CrossRef](#)] [[PubMed](#)]

17. Ruyters, S.; Mertens, J.; Vassilieva, E.; Dehandschutter, B.; Poffijn, A.; Smolders, E. The red mud accident in Ajka (Hungary): Plant toxicity and trace metal bioavailability in red mud contaminated soil. *Environ. Sci. Technol.* **2011**, *45*, 1616–1622. [[CrossRef](#)] [[PubMed](#)]
18. Alves, L. Toxic water seeps from Norwegian mining site in Brazil's Amazon. The Rio Times, 2018. Available online: <https://www.riotimesonline.com/brazil-news/rio-politics/toxic-water-seeps-from-norwegian-mining-site-in-brazils-amazon/> (accessed on 2 February 2024).
19. Kuntikana, G.; Singh, D.N. Contemporary issues related to utilization of industrial byproducts. *Adv. Civ. Eng. Mater.* **2017**, *6*, 444–479. [[CrossRef](#)]
20. Kong, X.; Guo, Y.; Xue, S.; Hartley, W.; Wu, C.; Ye, Y.; Cheng, Q. Natural evolution of alkaline characteristics in bauxite residue. *J. Clean. Prod.* **2017**, *143*, 224–230. [[CrossRef](#)]
21. Hua, Y.; Heal, K.V.; Friesl-Hanl, W. The use of red mud as an immobiliser for metal/metalloid-contaminated soil: A review. *J. Hazard. Mater.* **2017**, *325*, 17–30. [[CrossRef](#)] [[PubMed](#)]
22. Dodoo-Arhin, D.; Nuamah, R.A.; Agyei-Tuffour, B.; Obada, D.O.; Yaya, A. Awaso bauxite red mud-cement based composites: Characterisation for pavement applications. *Case Stud. Constr. Mater.* **2017**, *7*, 45–55. [[CrossRef](#)]
23. Metecan, I.H.; Karayildirim, T.; Yanik, J.; Saglam, M.; Yuksel, M. The effect of sulfur-promoted red mud catalysts on hydroliquefaction of oil shale. *Oil Shale* **2003**, *20*, 69–79. [[CrossRef](#)]
24. Mastral, A.; Mayoral, C.; Izquierdo, M.; Pardos, C. Iron-catalyzed hydrogenation of high-sulfur content coals. *Fuel Process. Technol.* **1993**, *36*, 177–184. [[CrossRef](#)]
25. Yokoyama, S.; Yamamoto, M.; Maekawa, Y.; Kotanigawa, T. Catalytic activity of sulphate for hydroliquefaction of coal by using diphenylether and diphenylmethane. *Fuel* **1989**, *68*, 531–533. [[CrossRef](#)]
26. Vangelatos, I.; Angelopoulos, G.N.; Boufounos, D. Utilization of ferroalumina as raw material in the production of Ordinary Portland Cement. *J. Hazard. Mater.* **2009**, *168*, 473–478. [[CrossRef](#)] [[PubMed](#)]
27. Tang, W.C.; Wang, Z.; Liu, Y.; Cui, H.Z. Influence of red mud on fresh and hardened properties of self-compacting concrete. *Constr. Build. Mater.* **2018**, *178*, 288–300. [[CrossRef](#)]
28. Chen, Y.; Ke, Y.; Liang, S.; Hu, J.; Hou, H.; Yang, J. Enhanced bromine fixation and tar lightweighting in co-pyrolysis of non-metallic fractions of waste printed circuit boards with Bayer red mud. *Waste Manag.* **2023**, *162*, 72–82. [[CrossRef](#)] [[PubMed](#)]
29. Kang, K.; Loeb sack, G.; Sarchami, T.; Klinghoffer, N.B.; Papari, S.; Yeung, K.K.-C.; Berruti, F. Production of a bio-magnetic adsorbent via co-pyrolysis of pine wood waste and red mud. *Waste Manag.* **2022**, *149*, 124–133. [[CrossRef](#)] [[PubMed](#)]
30. Li, Y.; Min, X.; Ke, Y.; Liu, D.; Tang, C. Preparation of red mud-based geopolymer materials from MSWI fly ash and red mud by mechanical activation. *Waste Manag.* **2019**, *83*, 202–208. [[CrossRef](#)] [[PubMed](#)]
31. Occhicone, A.; Vukčević, M.; Bosković, I.; Ferone, C. Red Mud-Blast Furnace Slag-Based Alkali-Activated Materials. *Sustainability* **2021**, *13*, 11298. [[CrossRef](#)]
32. Consoli, N.C.; Párraga Morales, D.; Saldanha, R.B. A new approach for stabilization of lateritic soil with Portland cement and sand: Strength and durability. *Acta Geotech.* **2021**, *16*, 1473–1486. [[CrossRef](#)]
33. Kulkarni, P.P.; Mandal, J.N. Strength evaluation of soil stabilized with nano silica-cement mixes as road construction material. *Constr. Build. Mater.* **2022**, *314*, 125363. [[CrossRef](#)]
34. Raja, K.; Venkatachalam, S.; Vishnuvardhan, K.; Siva Rama Krishnan, R.; Tamil Selvan, V.; Vetrivelan, N. A review on soil stabilization using rice husk ash and lime sludge. *Mater. Today Proc.* **2022**, *65*, 1205–1212. [[CrossRef](#)]
35. Andavan, S.; Pagadala, V.K. A study on soil stabilization by addition of fly ash and lime. *Mater. Today Proc.* **2020**, *22*, 1125–1129. [[CrossRef](#)]
36. Karami, H.; Pooni, J.; Robert, D.; Costa, S.; Li, J.; Setunge, S. Use of secondary additives in fly ash based soil stabilization for soft subgrades. *Transp. Geotech.* **2021**, *29*, 100585. [[CrossRef](#)]
37. Bulbul, S.; Ayhan, E.; Gökmeşe, H. Termik Santral Atığı Olan Kömür Külünün SBR Matrisli Bileşiklere İlave Edilmesinin Mekanik Özelliklere Etkisi. *Necmettin Erbakan Üniversitesi Fen Ve Mühendislik Bilim. Derg.* **2023**, *5*, 135–146.
38. National Academies of Sciences E and M (NASEM). *Recommended Practice for Stabilization of Subgrade Soils and Base Materials*; The National Academies Press: Washington, DC, USA, 2009.
39. Rao, C.; Naidu, P.G.; Satyanarayana, P.V.V.; Adishesu, S. Application of GGBS stabilized red mud in road construction. *IOSR J Eng.* **2012**, *2*, 14–20.
40. Ma, S.; Sun, Z.; Wei, J.; Zhang, X.; Zhang, L. Utilization of modified red mud waste from the bayer process as subgrade and its performance assessment in a large-sale application. *Coatings* **2022**, *12*, 471. [[CrossRef](#)]
41. Chen, R.; Cai, G.; Dong, X.; Mi, D.; Puppala, A.J.; Duan, W. Mechanical properties and micro-mechanism of loess roadbed filling using by-product red mud as a partial alternative. *Constr. Build. Mater.* **2019**, *216*, 188–201. [[CrossRef](#)]
42. Sahoo, S.; Mohanty, C. Construction of road sub-base by using industrial waste. *Int. J. Eng. Res. Dev.* **2016**, *3*, 20–26.
43. Kushwaha, S.S.; Kishan, D. Stabilization of red mud by lime and gypsum and investigating its possible use in geoenvironmental engineering. In Proceedings of the Geo-Chicago 2016, Chicago, IL, USA, 14–18 August 2016; pp. 978–988.
44. Sabat, A.K.; Mohanta, S. Efficacy of dolime fine stabilized red mud-fly ash mixes as subgrade material. *ARPN J. Eng. Appl. Sci.* **2015**, *10*, 5919–5923.
45. Satayanarayana, P.V.V.; Naidu, G.; Adishesu, S.; Rao, C. Characterization of lime stabilized red mud mix for feasibility in road construction. *Int. J. Eng. Res. Dev.* **2012**, *3*, 20–26.

46. ASTM D2487; Standard Practice for Classification of Soils for Engineering Purposes (Unified Soil Classification System). ASTM International: West Conshohocken, PA, USA, 2017.
47. Chen, C.R.; Phillips, I.R.; Wei, L.L.; Xu, Z.H. Behaviour and dynamics of di-ammonium phosphate in bauxite processing residue sand in Western Australia—I. NH₃ volatilisation and residual nitrogen availability. *Environ. Sci. Pollut. Res.* **2010**, *17*, 1098–1109. [[CrossRef](#)] [[PubMed](#)]
48. Santini, T.C.; Fey, M.V. Spontaneous Vegetation Encroachment upon Bauxite Residue (Red Mud) As an Indicator and Facilitator of In Situ Remediation Processes. *Environ. Sci. Technol.* **2013**, *47*, 12089–12096. [[CrossRef](#)] [[PubMed](#)]
49. ASTM C618-17; Standard Specification for Coal Ash and Raw or Calcined Natural Pozzolan for Use in Concrete. ASTM International: West Conshohocken, PA, USA, 2018.
50. ASTM C618-23; Standard Specification for Coal Ash and Raw or Calcined Natural Pozzolan for Use in Concrete. ASTM International: West Conshohocken, PA, USA, 2023.
51. Zha, F.; Liu, S.; Du, Y.; Cui, K. Behavior of expansive soils stabilized with fly ash. *Nat. Hazards* **2008**, *47*, 509–523. [[CrossRef](#)]
52. Yenginar, Y.; Olgun, M. Optimizing installation parameters of DM columns in clay using Taguchi method. *Bull. Eng. Geol. Environ.* **2023**, *82*, 145. [[CrossRef](#)]
53. Yenginar, Y.; Olgun, M. Optimizing construction parameters of DMC in high plasticity soils. In Proceedings of the 8th Geotechnical Symposium, İstanbul, Turkey, 13–15 November 2019.
54. ASTM D4318; Standard Test Methods for Liquid Limit, Plastic Limit, and Plasticity Index of Soils. ASTM International: West Conshohocken, PA, USA, 2017.
55. ASTM D698-12; Standard Test Methods for Laboratory Compaction Characteristics of Soil Using Standard Effort (12,400 ft-lbf/ft³ (600 kN-m/m³)) [Internet]. ASTM International: West Conshohocken, PA, USA, 2021.
56. ASTM D2166; Standard Test Method for Unconfined Compressive Strength of Cohesive Soil. ASTM International: West Conshohocken, PA, USA, 2016.
57. ASTM D1883-21; Standard Test Method for California Bearing Ratio (CBR) of Laboratory-Compacted Soils. ASTM International: West Conshohocken, PA, USA, 2021.
58. Sarath Chandra, K.; Krishnaiah, S. Strength and leaching characteristics of red mud (bauxite residue) as a geomaterial in synergy with fly ash and gypsum. *Transp. Res. Interdiscip. Perspect.* **2022**, *13*, 100566. [[CrossRef](#)]
59. HTS. *Highway Technical Specification*; General Directorate of Highways: Ankara, Turkey, 2013.

Disclaimer/Publisher's Note: The statements, opinions and data contained in all publications are solely those of the individual author(s) and contributor(s) and not of MDPI and/or the editor(s). MDPI and/or the editor(s) disclaim responsibility for any injury to people or property resulting from any ideas, methods, instructions or products referred to in the content.